

NBI Heating Analysis of Time-Development Plasma in LHD^{*})

Hiroyuki YAMAGUCHI, Sadayoshi MURAKAMI, Arimitsu WAKASA, Akira SAKAI, Atsushi FUKUYAMA, Masaki OSAKABE¹⁾, Hiromi TAKAHASHI¹⁾, Ichihiko YAMADA¹⁾ and LHD experimental group¹⁾

Department of Nuclear Engineering, Kyoto University, Sakyo-ku, Kyoto 606-8501, Japan

¹⁾*National Institute for Fusion Science, Toki 509-5292, Japan*

(Received 7 December 2012 / Accepted 26 April 2013)

A neutral beam injection heating simulation of time-development plasma in the Large Helical Device high-ion-temperature experiment is presented. The effects of the time-development of density and temperature on the beam ion birth profile and slowing-down are considered using a new code, GNET-TD, which is based on GNET. The simulation results show that heat deposition to ions increases in the core region when the density decays after pellet injection.

© 2013 The Japan Society of Plasma Science and Nuclear Fusion Research

Keywords: LHD, NBI heating, time-development plasma, GNET

DOI: 10.1585/pfr.8.2403099

1. Introduction

Extending of the high-temperature region in helical systems is important for obtaining a better understanding of the physics properties of high-temperature plasmas in non-axisymmetric devices. In the Large Helical Device (LHD), high-ion-temperature (high- T_i) experiment was conducted by neutral beam injection (NBI) heating and carbon impurity pellet injection [1, 2]. In the high- T_i experiment plasma, the density and temperature rapidly changed with time because of pellet injection, and an increase in the ion temperature was observed in the decay phase of density. To understand the transport properties of this time-development plasma, accurate information of power deposition by NBI during discharge is necessary.

The power deposition by NBI heating is affected by the drift motion of the beam ions during slowing-down. On the other hand, in helical systems, drift orbits of energetic particles are complicated due to the three-dimensional (3D) effect of the magnetic configurations. Further, in tokamaks, toroidal ripples exist because of the finite number of toroidal field coils and may enhance energetic particle transport. Several tokamak simulations have been used orbit-following Monte Carlo codes such as ASCOT [3] in EURATOM and OFMC [4] in JAEA. However, those codes cannot treat a full 3D field. GNET is a Monte Carlo code that has been widely used in the analysis of LHD plasmas, for example, electron cyclotron, NBI, and ion cyclotron resonance frequency heating [5–7]. However, the conventional version of GNET can treat only steady-state plasmas.

In this study, we develop a new code based on GNET,

GNET-TD, which considers the time development of the density and temperature of the background plasma. The new code is applied to an NBI heating simulation of the time-development plasma in the LHD high- T_i experiment. In the next section, we describe the physical model used in GNET and the improvements made for application to time-development plasmas. In section 3, we discuss the simulation results. The final section discusses the conclusion.

2. Simulation Models

In NBI heating analysis, the conventional version of GNET solves a drift kinetic equation in a five-dimensional phase space (three dimensions in real space and two in velocity space)

$$\begin{aligned} \frac{\partial f_{\text{beam}}}{\partial t} + (\mathbf{v}_{\parallel} + \mathbf{v}_D) \cdot \nabla f_{\text{beam}} + \dot{\mathbf{v}} \cdot \nabla_{\mathbf{v}} f_{\text{beam}} \\ = C^{\text{coll}}(f_{\text{beam}}) + L^{\text{particle}}(f_{\text{beam}}) + S, \end{aligned} \quad (1)$$

by the Monte Carlo method. Here f_{beam} is the distribution function of the beam ions, \mathbf{v}_{\parallel} is the velocity parallel to the field line, \mathbf{v}_D is the drift velocity, C^{coll} is the linear Coulomb collision operator, L^{particle} is the particle loss term, and S is the time-independent source term evaluated by FIT3D [8]. The guiding center orbits of test particles are expressed in Boozer coordinates and followed by 6th order Runge-Kutta method. The steady-state solution for f_{beam} is obtained by the convolution integral of the test particle distributions with respect to time during slowing-down.

In a time development plasma, in which the density and temperature change with time, the source term S in Eq. (1) becomes time-dependent, because the birth profile of the beam ions depends on density and temperature. In addition, during slowing-down, the beam ions undergo a

author's e-mail: yamaguchi@p-grp.nucleng.kyoto-u.ac.jp

^{*}) This article is based on the presentation at the 22nd International Toki Conference (ITC22).

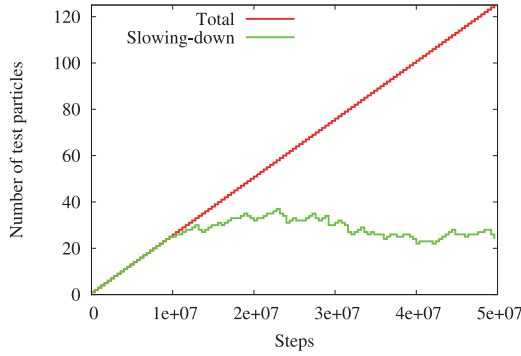


Fig. 1 Number of test particles on one typical core in an NBI heating simulation by GNET-TD using 4000 cores with the removal routine. Red line indicates total number of test particles that have started to slow down. Green line indicates number of test particles that are slowing down.

change in the collision frequencies. In GNET-TD, the radial profiles of the density and temperature of the background plasma can be arbitrarily changed at each time step. Now the code is designed to read the fitted data of the radial profiles of n_e , T_e and T_i . In this study, we set the time step for the change in the background plasma profile to 2 ms. To introduce the time-dependent source term, the birth profiles of the beam ions are evaluated every 0.5 ms. This time step width is also used as the interval of integration of the test particle distribution with respect to time. These test particles are introduced into the drift motion and collision calculation routine sequentially.

In GNET-TD, a larger number of test particles are required than in GNET if we want to obtain the same level of statistical accuracy. To reduce the computation time, we introduce a routine that removes test particles that are lost or thermalized. We set the boundary energy of thermalized particles to $1.5T_i(\rho)$, where ρ denotes the radial position of the particle. Figure 1 shows the number of test particles on one typical core at each steps when we use 4000 cores with the removal routine. The green line indicates the number of test particles that are not lost or thermalized. By using this routine, we can reduce the computational time by about 50%.

We have done the benchmarking of GNET-TD by means of comparison with previous GNET. We ran the both codes under the same condition of a steady-state LHD plasma and NBI heating, and we confirmed that GNET-TD reproduces the results of GNET well.

3. Simulation Results

Using GNET-TD, we performed an NBI heating simulation of the high- T_i experiment in LHD. The shot number is 110597. Figure 2 shows the time evolution of shot number 110599, which is almost equivalent to 110597. The magnetic axis $R_{ax} = 3.6$ m and the field strength $B_0 = -2.85$ T. Here the minus sign indicates a reversed magnetic field configuration.

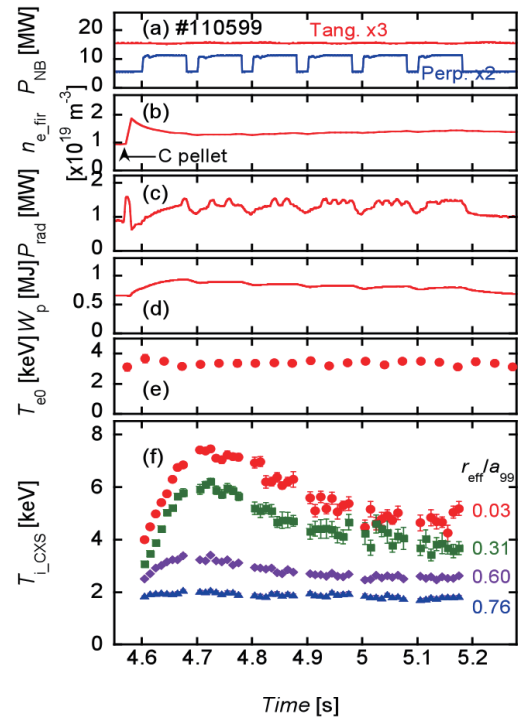


Fig. 2 Time evolution of (a) port-through power of NB, (b) electron density, (c) radiation power, (d) stored energy, (e) electron temperature, and (f) ion temperature in LHD high- T_i experiment (shot number 110599) [2].

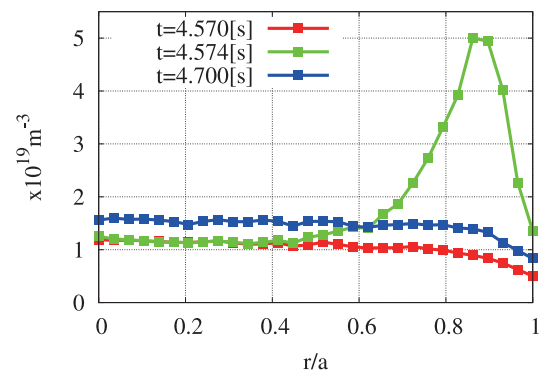


Fig. 3 Radial profiles of electron density at three different times in shot 110597.

The time evolution of n_e in this shot is shown in Fig. 2 (b). The rapid increase in the density at $t = 4.574$ s is due to pellet injection. Figure 3 shows the radial profiles of n_e at three different times. Here r/a is the normalized minor radius. The rapid increase in the density occurs in the outer region of the plasma, and the density slowly increases in the core region. In this study, we assume that the background plasma is a pure hydrogen plasma, and the effect of carbon impurities is not considered. The beam energy is ~ 180 keV for tangential NB#1-3 and ~ 40 keV for perpendicular NB#4-5. The injection powers of NB#1-5 are set to 5.66, 4.55, 5.08, 5.50, and 5.60 MW, respectively. These

data are the input to FIT3D and GNET-TD.

We evaluated the birth profiles of the beam ions for each beam component using FIT3D. Figure 4 shows the deposition rate of neutral beams of NB#1 (tangential) and NB#5 (perpendicular) as a function of time. The deposition of the neutral beam changes in response to change in the electron density.

Figure 5 shows the beam-ion distribution functions in velocity space at $r/a = 0.8$ and $r/a = 0.2$. In these graphs, the left (right) corresponds to $t = 4.572$ (4.576) s just before (after) pellet injection. Here v_{\parallel} is the velocity parallel to the field line, v_{\perp} is the velocity perpendicular to the field line, and v_{th0} is the ion thermal velocity at $T_e = 4$ keV. A clear reduction in the high-energy part of the distribution appears at $r/a = 0.8$, when the pellet is injected. This can be interpreted as an enhancement of the slowing-down

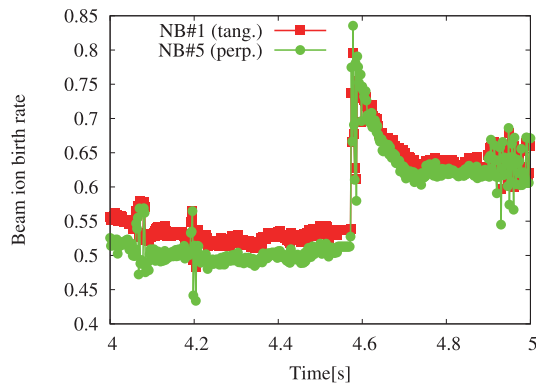


Fig. 4 Beam-ion birth rate of NB#1 and #5 as a function of time evaluated by FIT3D.

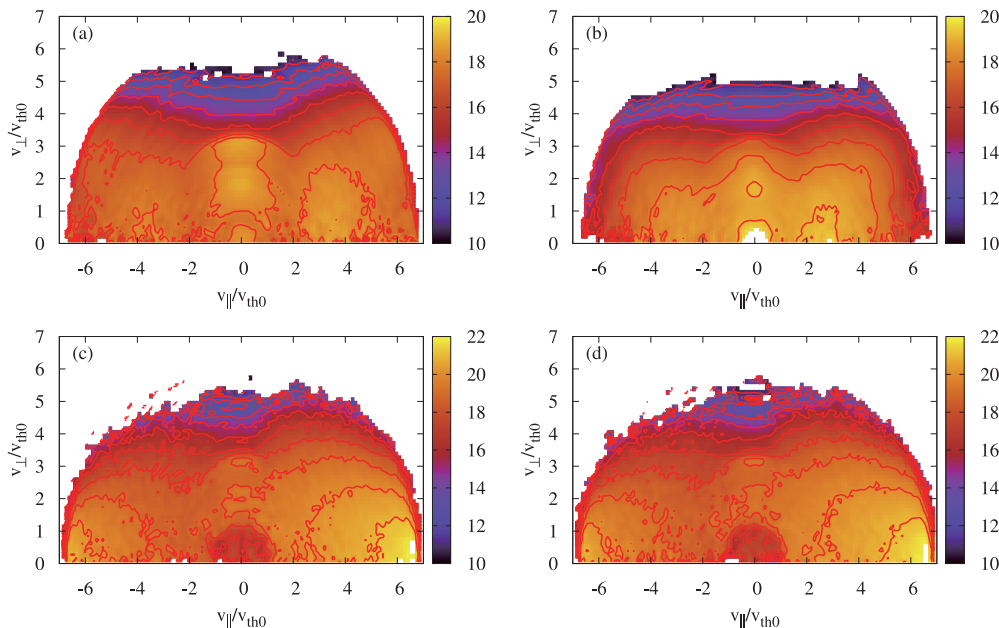


Fig. 5 Beam-ion distribution functions in velocity space at (a) $t = 4.572$ s, $r/a = 0.8$, (b) $t = 4.576$ s, $r/a = 0.8$, (c) $t = 4.572$ s, $r/a = 0.2$, and (d) $t = 4.576$ s, $r/a = 0.2$. A clear reduction in the high-energy component appears at $r/a = 0.8$.

caused by the increase in the density. On the other hand, no clear change appears in the beam-ion distribution at $r/a = 0.2$.

Figure 6 shows the volume-integrated power deposition to electrons (P_e) and to ions (P_i), and the total power deposition ($P_{total} = P_e + P_i$). A rapid change is seen due to the pellet at $t = 4.574$. Oscillation due to the modulation of NB#4 can be seen after $t = 4.6$ s. The power deposition becomes sufficiently steady state before pellet injection at $t = 4.574$ s. A rapid increase in the power deposition can be seen at $t = 4.574$ s; it is due to the rapid increase in the density caused by pellet injection.

The power deposition to electrons and ions volume-integrated over the core region ($r/a < 0.5$) is shown in Fig. 7. The electron and ion heating start to increase after pellet injection at $t = 4.574$ s. The ion heating reaches its

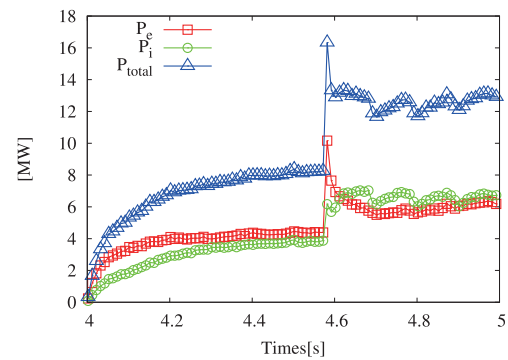


Fig. 6 Power deposition by NBI during shot 110597. P_e (P_i) represents the power deposition to electrons (ions).

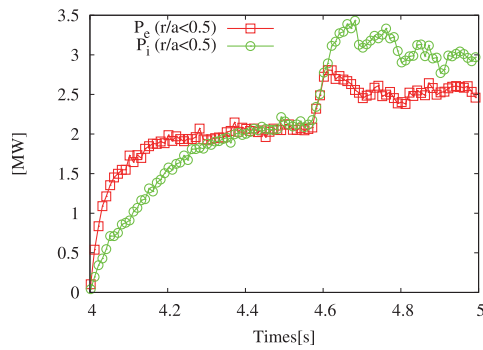


Fig. 7 Heating power to electrons and ions volume-integrated in core region, $r/a < 0.5$.

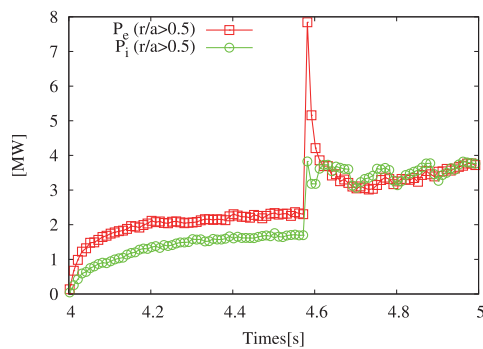


Fig. 8 Heating power to electrons and ions volume-integrated in outer region, $r/a > 0.5$.

maximum value at $t = 4.69$ s. After $t = 4.6$ s, ion heating becomes greater than electron heating. This is because the injection of NB#4 starts at $t = 4.6$ s with a beam energy of 40 keV.

Figure 8 shows the power deposition in the outer region ($r/a > 0.5$). The heating in the outer region rapidly changes. The electron heating reaches a local minimum after a sharp decay due to the reduction in the high-energy component of the beam ions. In contrast, the ion heating exhibits a step-like increase.

Figure 9 shows the radial distributions of P_i per volume at three different times. At pellet injection ($t = 4.574$ s), the ion heating increases only in the outer region, $r/a \sim 0.7-1.0$. The ion heating in the core region increases in the decay phase of the electron density.

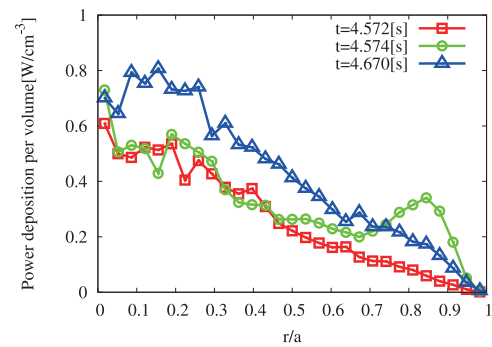


Fig. 9 Radial distributions of power deposition to ions at three different times.

4. Summary

We have developed the GNET-TD code, which is based on the GNET code and considers the time development of the density and temperature of the background plasma. We applied GNET-TD to an NBI heating simulation of the LHD high- T_i experiment. The simulation results show the changes in the beam ion distribution functions and power deposition due to pellet injection. These results reveal that the power deposition by NBI increases when the pellet is injected. Evaluating the radial distribution of the heating power, we found that the heat deposition increases in the core in the decay phase of the density, whereas the power deposition rapidly increases in the outer region.

In the future, we will perform a heat transport simulation using the results of the heating power calculated by GNET-TD. In addition, to validate our simulation code, we will compare our simulation results with experimental observations measured using CX-NPA or other measurement system.

- [1] K. Nagaoka *et al.*, Nucl. Fusion **51**, 083022 (2011).
- [2] H. Takahashi *et al.*, Proc. 24th IAEA-FEC, San Diego, 2012, EX/2-5.
- [3] J.A. Heikkinen and S.K. Sipilä, Phys. Plasmas **2**, 3724 (1995).
- [4] K. Shinohara *et al.*, Nucl. Fusion **43**, 586 (2003).
- [5] S. Murakami *et al.*, Nucl. Fusion **40**, 693 (2000).
- [6] S. Murakami *et al.*, Sci. Technol. **46**, 241 (2004).
- [7] S. Murakami *et al.*, Nucl. Fusion **46**, S425 (2006).
- [8] S. Murakami *et al.*, Fusion Technol. **27**, Suppl. S, 256 (1995).